

Ultrafast relaxation of photoexcited superfluid He nanodroplets

M. Mudrich

Department of Physics and Astronomy, Aarhus University, Denmark

A. LaForge^{*} and F. Stienkemeier

Institute of Physics, University of Freiburg, Germany

A. Ciavardini,[†] P. O’Keeffe, and M. Coreno

CNR-ISM, Area della Ricerca di Roma 1, Monterotondo Scalo, Italy

Y. Ovcharenko[‡] and T. Möller

Institut für Optik und Atomare Physik, TU-Berlin, Germany

M. Ziemkiewicz

*Ultrafast X-ray Science Laboratory, Chemical Sciences Division,
Lawrence Berkeley National Laboratory, Berkeley, USA,
and Department of Chemistry, University of California, USA*

M. Devetta[§] and P. Piseri

Dipartimento di Fisica, Università degli Studi di Milano, Milan, Italy

M. Drabbels

Federal Institute of Technology Lausanne (EPFL), Switzerland

A. Demidovich, C. Grazioli, P. Finetti, O. Plekan, M. Di Fraia, K. C. Prince, R. Richter, and C. Callegari

Elettra-Sincrotrone Trieste S.C.p.A., Italy

J. Eloranta

Department of Chemistry and Biochemistry, California State University at Northridge, USA

A. Hernando

*Kido Dynamics, EPFL Innovation Park Bat. C, CH-1015 Lausanne, Switzerland and
IFISC (CSIC-UIB), Instituto de Física Interdisciplinar y Sistemas Complejos,
Campus Universitat de les Illes Balears, E-07122 Palma de Mallorca, Spain*

M. Pi

*Departament FQA, Facultat de Física, Universitat de Barcelona, Spain and
Institute of Nanoscience and Nanotechnology (IN2UB), Universitat de Barcelona, Spain*

M. Barranco

*Laboratoire des Collisions, Agrégats, Réactivité, IRSAMC, UMR 5589,
CNRS et Université Paul Sabatier-Toulouse 3, Toulouse Cedex 09, France
Departament FQA, Facultat de Física, Universitat de Barcelona, Spain and
Institute of Nanoscience and Nanotechnology (IN2UB), Universitat de Barcelona, Spain*

(Dated: May 14, 2019)

The relaxation of photoexcited nanosystems is a fundamental process of light-matter interaction. Depending on the couplings of the internal degrees of freedom, relaxation can be ultrafast, converting electronic energy in a few fs, or slow, if the energy is trapped in a metastable state that decouples from its environment. Here, helium nanodroplets are resonantly excited by femtosecond extreme-ultraviolet (XUV) pulses from a seeded free-electron laser. Despite their superfluid nature, we find that helium nanodroplets in the lowest electronically excited states undergo ultrafast relaxation. By comparing experimental photoelectron spectra with time-dependent density functional theory simulations, we unravel the full relaxation pathway: Following an ultrafast interband transition, a void nanometer-sized bubble forms around the localized excitation (He^*) within 1 ps. Subsequently, the bubble collapses and releases metastable He^* at the droplet surface. This study highlights the high level of detail achievable in probing the photodynamics of nanosystems using tunable XUV pulses.

Understanding the ultrafast response of condensed phase nanosystems to photoexcitation is essential for many research areas, including atmospheric science [1], radiation damage in biological matter [2, 3], light-harvesting mechanisms in natural and artificial complexes [4, 5], and photocatalysis [6]. However, the complex couplings of electronic and translational degrees of freedom often present major theoretical challenges [7]. In addition, the complexity of heterogeneous solid or liquid systems, as well as difficulties in preparing well-controlled samples and performing reproducible measurements, make it difficult to unravel the elementary steps in the relaxation process. In this respect, superfluid He nanodroplets are ideal model systems for studying the photodynamics in weakly-bound nanostructures, both experimentally and theoretically; He atoms have a simple electronic structure, interatomic binding is extremely weak, and, the structure of He nanodroplets is homogeneous and nearly size-independent due to their superfluid nature [8, 9]. Exploring transient phenomena associated with superfluidity is a particularly intriguing aspect of He nanodroplet spectroscopy [10, 11]. By probing the dynamics of laser-excited molecular systems coupled to He droplets, one gains insight into the fluid dynamics, dissipation, and transport properties of a superfluid on the molecular scale [12–14].

The properties of pure He droplets can be directly studied using electron bombardment or XUV radiation. From previous theoretical [15, 16] and static photoexcitation studies [17–23], the following dynamical response to resonant absorption of an XUV photon has been inferred: The electronic excitation created in the droplet localizes on an atomic or molecular center He_n^* , $n = 1, 2, \dots$, within a few 100 fs [24]. Subsequently, a void cavity or bubble forms around He_n^* due to Pauli repulsion between the excited electron and the surrounding ground state He atoms [21], which expands up to a radius of 6.4 Å [25] within about 350 fs [26]. Depending on how close to the droplet surface the excitation localizes, the bubble either collapses before fully forming thereby ejecting He^* or He_2^* out of the droplet, or remains in a metastable state in the droplet [21]. Using laser-based high-harmonic light sources [27], various ultrafast processes initiated by exciting high-lying states in the autoionization continuum of He nanodroplets have been revealed, including the emission of slow electrons [22], the ejection of Rydberg atoms and excimers [28, 29], and ultrafast interband relaxation [23]. However, the dynamics of low-lying states below the autoionization threshold and in particular the bubble formation have not been probed for pure He nanodroplets, neither at the strongest absorption band associated with the atomic $\text{He}^* 1s2p^1P$ state (photon energy around $h\nu = 21.6$ eV [18]), nor at the lowest optically accessible $1s2s^1S$ state ($h\nu = 21.0$ eV [18]).

In the present study we excite these lowest excited states to directly probe the relaxation dynamics of neu-

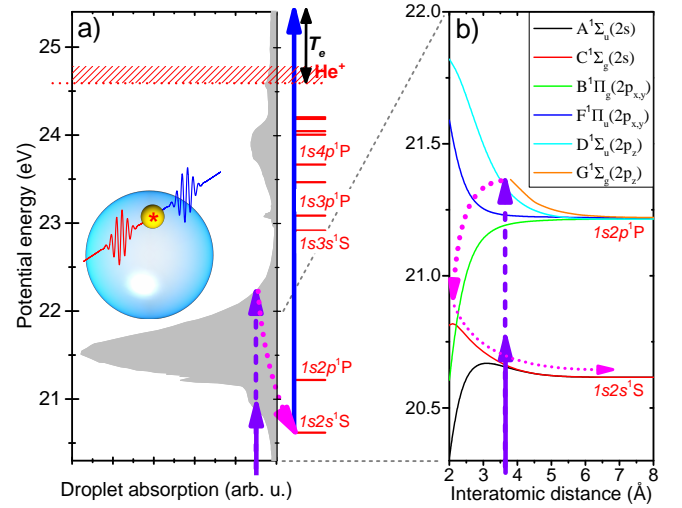


FIG. 1. Illustration of the pump-probe scheme. a) The filled area represents the absorption spectrum of He nanodroplets taken from Ref. [18]. He atomic levels are shown on the right-hand side. b) Potential curves of the singlet-excited He_2^* dimer correlating to the $1s2s^1S$ and $1s2p^1P$ atomic states (see Methods section). The vertical straight arrows indicate the pump and probe laser pulses, the dotted curved arrows indicate the droplet relaxation pathway. The double-sided arrow in a) illustrates the electron kinetic energy T_e .

tral pure He nanodroplets. The experiment was carried out using tunable XUV pulses generated by the seeded free-electron laser (FEL) FERMI [30]. The comparison of time-resolved photoelectron spectra (PES) with time-dependent density functional theory (TD-DFT) calculations reveals an ultrafast three-step relaxation process. Despite the extremely weak binding of the He atoms in the droplets and the superfluid nature thereof, energy dissipation is very efficient even for the lowest excited states; more than 1 eV of electron energy is dissipated in less than 1 ps due to the coupling of electronic and nanofluid nuclear degrees of freedom.

The pump-probe scheme is sketched in Fig. 1. The gray shaded area in a) shows the absorption spectrum of He nanodroplets taken from Ref. [18]; for reference, the He^* atomic levels are given on the right-hand side of Fig. 1 a). The massive broadening and shifting of the atomic-like excited state is due to unfavorable Rydberg-core interaction [31]. The straight vertical arrows illustrate the pump (purple) and probe (blue) steps, realized by one XUV pulse and one time delayed UV pulse. The electron kinetic energy, T_e , measured by means of electron velocity-map imaging (VMI) [30, 32], is indicated as a black double-sided arrow. The most likely relaxation pathway for $1s2p^1P$ -excited He nanodroplets is indicated by the dotted curved arrows. The inset shows a schematic view of a He nanodroplet exposed to a pair of laser pulses, containing a localized excitation marked by

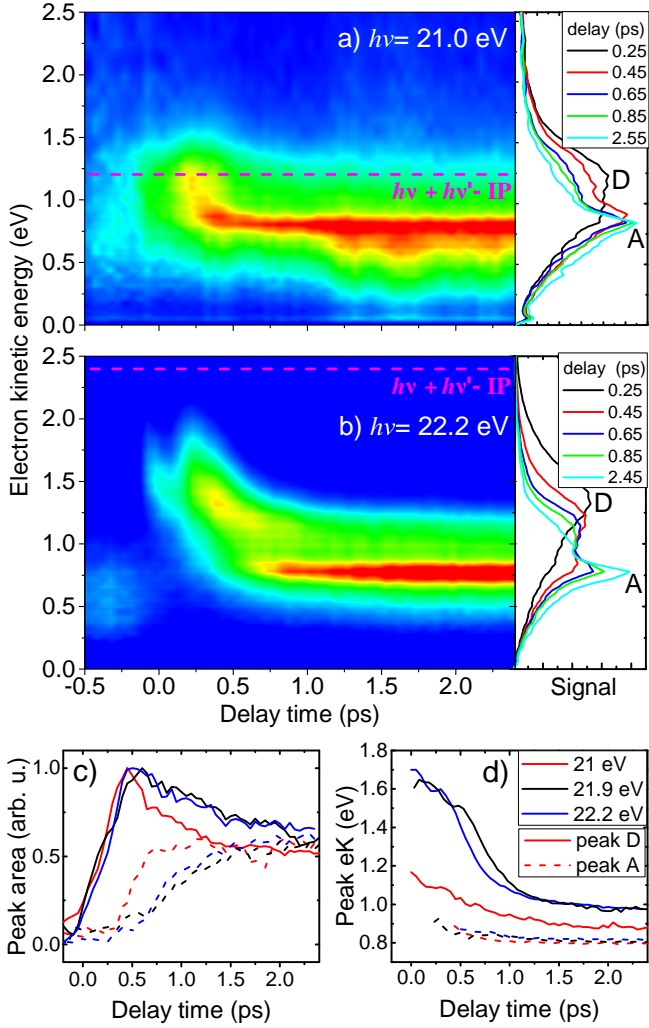


FIG. 2. Time-resolved photoelectron spectra of He nanodroplets containing on average $\bar{N} = 5 \times 10^5$ He atoms excited to their $1s2s$ state at the pump photon energy $h\nu = 21.0$ eV (a) and the $1s2p$ state at $h\nu = 22.2$ eV (b). The probe photon energy is $h\nu' = 4.8$ eV. The horizontal dashed lines indicate the electron energy corresponding to direct two-photon ionization of He. The panels on the right-hand sides show the electron spectra recorded at various fixed pump-probe delays. The bottom panels show the results of fitting the spectra with multiple peaks [area in c), position in d)].

(*)).

Examples of time-dependent PES measured by exciting He droplets to the $1s2s^1S$ state ($h\nu = 21.0$ eV) and on the blue edge of the $1s2p^1P$ band ($h\nu = 22.2$ eV) are shown in Fig. 2 a) and b), respectively. The horizontal dashed lines indicate the electron energy one would expect for direct $1+1'$ ionization of He by absorption of one pump and one probe photon, $T_e^{\text{direct}} = h\nu + h\nu' - E_i$, where $E_i = 24.6$ eV is the ionization energy of He and $h\nu' = 4.8$ eV is held fixed. The panels on the right-hand sides show the PES at selected pump-probe delays. For positive delays (XUV first, UV second), the PES mainly

consist of two spectral components in both cases a) and b). A broad feature labeled ‘D’ dominates the PES at short delays $t \lesssim 0.5$ ps, whereas a sharp peak ‘A’ becomes prominent at longer delays. Figs. 2 c) and d) show the amplitudes and center positions of these two peaks obtained from fits of the PES measured at various $h\nu$ (see Methods section). Peak D [solid lines in Fig. 2 c)] rises within the first 0.5 ps delay time and then slowly decreases, accompanied by a rapid increase of peak A (dashed lines). The opposite trends of these two components indicates a redistribution of population from D to A within 0.5-2.5 ps.

The energy of peak D [Fig. 2 d)] rapidly decreases within $t < 1$ ps, followed by a slow decrease beyond 2.5 ps. Peak A slightly shifts from 0.9 to 0.8 eV within $t < 1$ ps and remains constant thereafter. This value matches the electron energy expected for ionization of a He atom in the lowest excited singlet state, $T_e^{\text{atom}} = E(1s2s^1S) + h\nu' - E_i = 0.8$ eV, where $E(1s2s^1S) = 20.6$ eV. Therefore, we associate peak A with the ionization of a $1s2s^1S$ -excited He^* which is either weakly bound to the droplet surface or ejected into vacuum. This interpretation is supported by PES measured for various He droplet sizes presented in the supplementary material (SM). While for larger droplets peak A appears slightly later and remains less intense in proportion to peak D, its position converges to the same final value (0.8 eV). Consequently, peak D is assigned to a He^* located further inside the He droplet such that it is energetically shifted up. When exciting the He droplet to its $1s2s^1S$ state [Fig. 2 a)], the initial position of peak D (1.2 eV) matches the electron energy one expects based on the droplet absorption spectrum [Fig. 1 a)], $T_e^{\text{drop}} = 21 \text{ eV} + h\nu' - E_i = 1.3$ eV. At higher $h\nu$, where mainly the $1s2s^1P$ droplet state is excited [Fig. 2 b)], feature D corresponds to a superposition of 1S and 1P states which relaxes into the 1S droplet state faster than the cross correlation of the two laser pulses (250 fs FWHM) and thus cannot be fully resolved. Note that not all droplets evolve into the atomic 1S state (peak A), but nearly the same fraction of atoms remain in feature D which converges to an energy 0.1-0.2 eV above the 1S atomic value.

How can the extremely weakly bound, ultracold van der Waals He clusters induce ultrafast energy relaxation by up to 1.6 eV within 1 ps? To answer this question, we first consider the potential curves of the He_2^* excimer correlated to the atomic $1s2s^1S$ and $1s2p^1P$ levels as the simplest model system for the excited He droplet, shown in Fig. 1 b). The blue-shifted absorption profiles with respect to the atomic levels can be related to the steep upwards bending of the optically active A , D and F states in the range of most probable interatomic distances (3.6 Å). Following excitation of the $1s2p^1P$ -correlated droplet state, ultrafast internal conversion proceeds due to level crossings at short interatomic distance

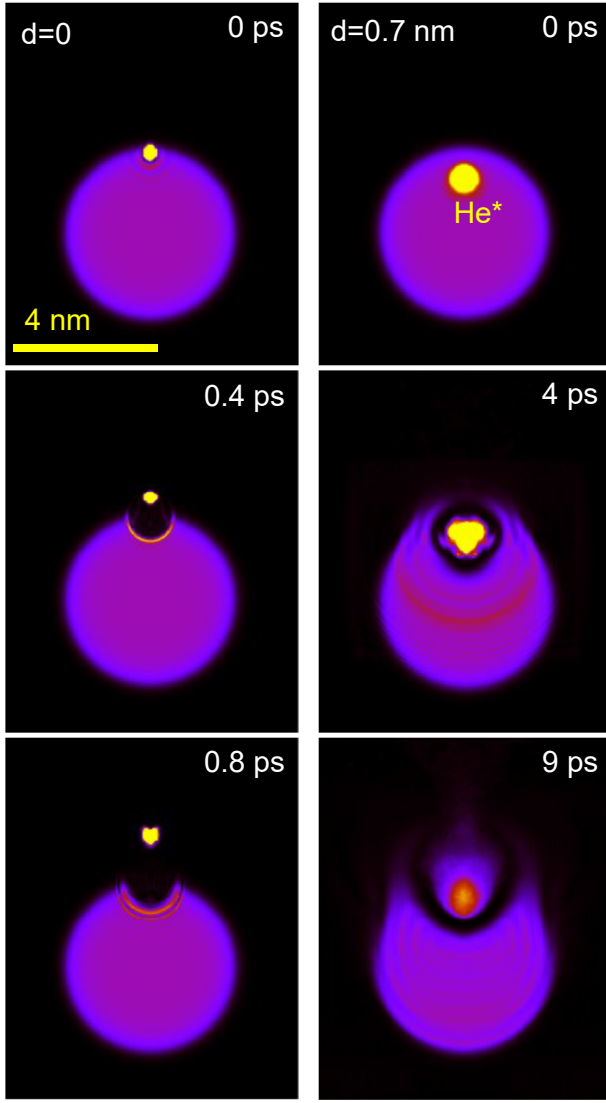


FIG. 3. Evolution of the simulated He density distribution and of the probability distribution of He^* (yellow dot) for an initial position of the He^* at 0 (left column) and at 0.7 nm (right column) away from the droplet surface.

according to the pathway indicated by the pink dotted arrows. Subsequently, the local environment rearranges to accommodate the newly formed $1s2s^1S$ He^* atom. On the longer timescale of the fluorescence lifetime, part of the He^* stabilize by forming He_2^* excimers [19, 20, 33].

To simulate this process for He droplets in three dimensions, we carried out TD-DFT calculations for a He^* excitation in the $1s2s^1S$ state, as outlined in the Methods section. Note that this transition is forbidden in free atoms. Therefore it preferentially takes place in the surface region of the droplets where the radially-varying He density breaks the symmetry of the free He atom and makes the transition partly allowed (see Methods).

As seen in Fig. 3, the system evolves differently depending on the initial position d of He^* with respect to

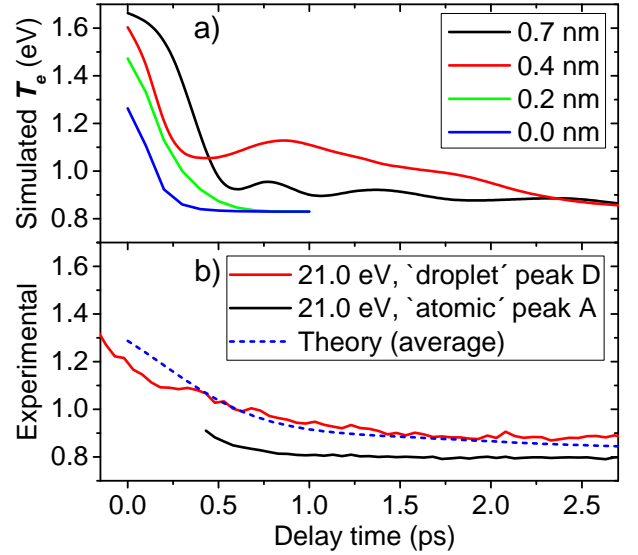


FIG. 4. Comparison between simulated (a) and measured (b) electron energies for droplet excitation of the $1s2s$ state at $h\nu = 21.0$ eV. The dashed line in b) is the average of the simulated curves in (a) taking into account their geometric weight as well as the experimental pulse cross correlation function.

the droplet surface. The radius of the droplet containing $N = 1000$ He atoms is 2.2 nm. Shown are snapshots of the He density distribution at fixed times t after He^* excitation. Animations of these simulations for various d are presented in the SM. When He^* is initially placed at the surface of the droplet ($d = 0$, left column), the surrounding region is locally compressed and forms a spherical dimple, while He^* flies off within $t \lesssim 1$ ps. This scenario resembles the dynamics of excited alkali metal atoms which initially reside in dimple states at the droplet surface [34–37]. When He^* is initially placed deeper in the bulk of the droplet ($d = 0.7$ nm, right column), first a bubble forms around He^* , which then bursts at $t \approx 4$ ps, thereby allowing He^* to escape out of the droplet. This scenario has been studied theoretically for photoexcited silver atoms [38], and experimentally for indium atoms embedded in He nanodroplets [14].

Besides visualizing the dynamics ensuing excitation of the droplet, the TD-DFT model allows us to simulate the time-dependent PES, see Methods section. Fig. 4 a) shows the resulting electron energies T_e^{sim} for different values of d . In the case He^* is initialized close to the droplet surface ($d = 0$ and 0.2 nm), T_e^{sim} rapidly drops from about 1.4 eV at $t = 0$ to the final value of 0.8 eV within $t = 250$ -500 fs due to prompt desorption of He^* . When He^* is placed deeper inside the droplet ($d = 0.4$ and 0.7 nm), an initial fast drop of T_e^{sim} from 1.6 to 0.9-1.1 eV is followed by a slow decrease to 0.9 eV at $t = 2$ ps.

The weighted average of these curves is shown in Fig. 4 b) as a dashed line. It nicely follows the experimental curve for the droplet feature D [red solid line in Fig. 4

b)] up to about 2 ps delay and eventually converges to the final value of the atomic peak A. In particular, the fast drop between 0 and 1 ps coincides with the drop of peak D energy in the experimental PES [Fig. 2 d)] and with the appearance of peak A as the bubble forms around He^* . Thereafter it slowly decreases from 0.9 to 0.8 eV as the bubble migrates to the droplet surface and eventually releases an unperturbed He^* . Note that the simulated curve for $d = 0.7$ nm shows an oscillatory behavior between $t = 0.4$ and 2 ps. We attribute this nearly periodic modulation of T_e to the oscillation of the He bubble around He^* . He bubble oscillations around impurity atoms (Ag and In) have also been discussed [14, 38].

From the comparison of the experimental and theoretical results we can now map out the full picture of the relaxation dynamics of excited He nanodroplets: Following $1s2p^1P$ excitation, ultrafast interband relaxation to the $1s2s^1S$ droplet state occurs within < 250 fs induced by curve crossings of the He_2^* potentials (step 1). This is in line with earlier photoluminescence studies which showed that the $1s2p^1P$ droplet state mainly decays by XUV-photon emission of He_2^* in its A state correlating to the $1s2s^1S$ state of He^* [19].

Further relaxation proceeds within the $1s2s^1S$ droplet band due to the local opening of a void bubble around He^* (step 2). The relaxation time associated with this step (0.5 ps) is in good agreement with the established model of bubble formation around an electron, if we assume a final bubble radius of 6.4 Å [25, 26]. It is nearly independent of the location of He^* within the droplet and of the droplet size \bar{N} . This explains the weak variation of the experimental pump-probe PES when changing \bar{N} .

Subsequently, the bubble migrates to the droplet surface and bursts to release a free He^* (step 3). The fact that in our experiment, both free and bubble-bound He^* are measured at $t = 2.5$ ps shows that the migration of the bubble to the surface is a slow process which strongly depends on the initial He^* location and therefore on \bar{N} . A recent study of the excited state dynamics of xenon clusters revealed electronic relaxation and the emission of free xenon atoms [39]. Thus, our findings appear not to be specific to He nanodroplets but of rather general relevance for weakly bound condensed phase systems. Eventually, the He^* that remain attached to the droplet surface further relax by forming He_2^* as seen in time-independent measurements [19, 20]. The latter radiatively decay to the ground state after undergoing vibrational relaxation and partly detaching from the droplet [33].

The presented measurements show that it is now possible to follow the relaxation dynamics of free nanodroplets in great detail using ultrashort tunable XUV pulses. This paves the way to probing the photodynamics of more complex natural or synthetic nanosystems in various regimes of excitation of the valence shell and even inner shells.

METHODS

The experiments described were performed at the Low Density Matter (LDM) end station of the seeded free-electron laser FERMI [30].

He droplet generation

The He nanodroplets were formed by expanding He gas from a high pressure reservoir (50 bar) through a pulsed, cryogenically cooled Even-Lavie nozzle at a pulse repetition rate of 10 Hz [40]. The mean size of the He droplets formed in this way was controlled by changing the temperature of the nozzle in the range of 5 to 28 K.

Light sources

Linearly polarized XUV pulses in the photon energy range 21.0-22.2 eV were provided by the FERMI free electron laser set to the 5th harmonic of the seed laser wavelength [41]. The XUV pulses generated in this way have a bandwidth < 0.1 eV and a temporal duration of about 100 fs FWHM. A Kirkpatrick-Baez mirror system was used to focus the FEL light to a spot size of 0.5 mm in the interaction region of the spectrometer. To minimize non-linear effects due to absorption of more than one photon per droplet the XUV pulses were strongly attenuated by a combination of a N_2 filled gas cell and an aluminum filter. The pulse energy in the interaction region was estimated to be 6 μJ .

The UV probe pulses (170 fs duration, 7 μJ pulse energy) were generated by frequency tripling part of the 775 nm Ti:Sa laser used to generate the seed light for the FEL. The UV pulses were focused to the same focal spot size as the XUV beam and superimposed with the XUV pulses in a quasi collinear geometry via reflection from a holey mirror. The temporal cross-correlation function was measured using two-photon ionization of He atoms *via* the He $1s5p^1P$ state. A Gaussian fit yields a FWHM of 250 fs.

Electron detection, data acquisition and analysis

PES from the He nanodroplets are recorded using a VMI spectrometer, in which electrons are accelerated by electrostatic imaging onto a position sensitive detector consisting of a 75 mm microchannel plate and phosphor screen assembly. For each step of the pump-probe delay of 50 fs delay, VMI spectrometer images from 2000 shots were saved. A background subtraction procedure was implemented in which the bunches of He nanodroplets were periodically desynchronized from the FEL pulses so that spurious signals such as scattered light could be

subtracted. The VMI spectrometer images for each delay were then summed and subsequently inverted using the pBasex routine to extract the photoelectron kinetic energy and angular distributions [42]. The PES for each value of the pump-probe delay were fit with a constrained 3 Gaussian fit. The time variation of the resulting fit parameters reveal the temporal behavior of the various ionization channels.

***Ab-initio* calculations of He-He* and He-He⁺ potentials and transition dipole moment**

The He*-He interaction potentials corresponding to $2s$ and $2p$ He atomic asymptotes were obtained at the CC3-EOM level [43, 44] by using the Psi4 code [45]. The basis set was taken from Ref. [46]. All the calculated potentials were corrected for basis set superposition errors by the counterpoise method of Boys and Bernardi [47].

The transition dipole $\vec{\mu}_{2s}$ as a function of He*($2s$)-He($1s$) distance was evaluated at the multi-reference configuration interaction (MRCI) level using the Molpro code [48, 49]. The active space consisted of the molecular states originating from $1s$ and $2s$ atomic states. These calculations employed the basis set given in Refs. [50] and [51]. The transition dipole induced by the inhomogeneous He density in the droplet surface region is calculated as the vector sum of dipole moments of a single He*-He pair weighted by the radial He density distribution,

$$\begin{aligned}\vec{\mu}_{2s}^{\text{drop}} &= \int d\mathbf{r} \rho(\mathbf{r}) \vec{\mu}_{2s}(|\mathbf{r} - \mathbf{r}_X|) \\ &= \int d\mathbf{r} \rho(\mathbf{r}) |\vec{\mu}_{2s}(|\mathbf{r} - \mathbf{r}_X|)| \frac{\mathbf{r} - \mathbf{r}_X}{|\mathbf{r} - \mathbf{r}_X|}.\end{aligned}\quad (1)$$

We find the transition dipole moment to be peaked nearly at the He droplet radius $r_0 N^{1/3}$, $r_0 = 2.22$ Å, where it takes the value $|\vec{\mu}_{2s}^{\text{drop}}| = 0.17$ Debye.

Time-dependent density function theory

The dynamics of the excited He droplet was simulated using time-dependent density functional theory (TD-DFT) for droplets consisting of 1000 He atoms [15, 16], to which the dynamics of the He* atom is self-consistently coupled.

Due to the light mass of the He* “impurity”, its dynamics is followed by solving the Schrödinger equation for it, where the potential term is given by the He*-droplet interaction. The expected high velocity of the impurity makes it advantageous to use the test-particles method for solving the Schrödinger equation [16, 34]. We obtain the excess energy transferred to the photoelectron as $T_e(t) = h\nu' - [U^+(t) - U^*(t)]$. Here, the interaction energies of He* with its local environment in the He droplet

in the (t -dependent) initial state, $U^*(t)$ is computed as

$$U^*(t) = \int \int d\mathbf{r} d\mathbf{r}' \Phi^2(\mathbf{r}', t) \rho(\mathbf{r}, t) \mathcal{V}_{\text{He-He}^*}(|\mathbf{r}' - \mathbf{r}|), \quad (2)$$

where Φ^2 is the probability density of He*, ρ is the ground-state He density, and $\mathcal{V}_{\text{He-He}^*}$ is the He-He* interaction pair potential, respectively. The interaction energy of He⁺ with the droplet in the final state, $U^+(t)$, is obtained in the same way only using the He-He⁺ interaction potential, $\mathcal{V}_{\text{He-He}^+}$.

Funding from the Deutsche Forschungsgemeinschaft (MU 2347/8-1, STI 125/19-1), Aarhus Universitets Forskningsfond, National Science Foundation (DMR-1828019), Carl-Zeiss-Stiftung, and Grant No. FIS2017-87801-P (AEI/FEDER, UE) is gratefully acknowledged.

* Now at Department of Physics, University of Connecticut, Storrs, Connecticut, USA

† Now at CERIC-ERIC Basovizza Trieste, Italy

‡ Now at European XFEL, Schenefeld, Germany

§ Now at CNR-IFN, Milano, Italy

- [1] C. George, M. Ammann, B. D’Anna, D. J. Donaldson, and S. A. Nizkorodov, *Chem. Rev.* **115**, 4218 (2015).
- [2] M. Barbatti, A. J. A. Aquino, J. J. Szymczak, D. Nachtigallova, P. Hobza, and H. Lischka, *PNAS* **107**, 21453 (2010).
- [3] K. Gokhberg, P. Kolorenč, A. I. Kuleff, and L. S. Cederbaum, *Nature* **505**, 661 (2014).
- [4] E. Collini, C. Y. Wong, K. E. Wilk, P. M. G. Curmi, P. Brumer, and G. D. Scholes, *Nature* **463**, 644 (2010).
- [5] H.-J. Son, S. Jin, S. Patwardhan, S. J. Wezenberg, N. C. Jeong, M. So, C. E. Wilmer, A. A. Sarjeant, G. C. Schatz, R. Q. Snurr, O. K. Farha, G. P. Wiederrecht, and J. T. Hupp, *J. Am. Chem. Soc.* **135**, 862 (2013).
- [6] J. Schneider, D. Bahnemann, J. Ye, G. L. Puma, and D. D. Dionysiou, *Photocatalysis: Fundamentals and Perspectives* (The Royal Society of Chemistry, Cambridge CB4 0WF, UK, 2016).
- [7] A. Masson, M.-C. Heitz, J.-M. Mestdag, M.-A. Gaveau, L. Poisson, and F. Spiegelman, *Phys. Rev. Lett.* **113**, 123005 (2014).
- [8] J. P. Toennies and A. F. Vilesov, *Angew. Chem. Int. Ed.* **43**, 2622 (2004).
- [9] F. Stienkemeier and K. Lehmann, *J. Phys. B* **39**, R127 (2006).
- [10] A. V. Benderskii, J. Eloranta, R. Zadayan, and V. A. Apkarian, *J. Chem. Phys.* **117**, 1201 (2002).
- [11] B. Grüner, M. Schlesinger, P. Heister, W. T. Strunz, F. Stienkemeier, and M. Mudrich, *Phys. Chem. Chem. Phys.* **13**, 6816 (2011).
- [12] N. B. Brauer, S. Smolarek, E. Loginov, D. Mateo, A. Hernando, M. Pi, M. Barranco, W. J. Buma, and M. Drabbels, *Phys. Rev. Lett.* **111**, 153002 (2013).
- [13] B. Shepperson, A. A. Søndergaard, L. Christiansen, J. Kaczmarczyk, R. E. Zillich, M. Lemesko, and H. Stapelfeldt, *Phys. Rev. Lett.* **118**, 203203 (2017).
- [14] B. Thaler, S. Ranftl, P. Heim, S. Cesnik, L. Treiber, R. Meyer, A. Hauser, W. Ernst, and M. Koch, *Nature Comm.* **9**, 4006 (2018).

- [15] M. Barranco, R. Guardiola, S. Hernández, R. Mayol, J. Navarro, and M. Pi, *J. Low Temp. Phys.* **142**, 1 (2006).
- [16] F. Ancilotto, M. Barranco, F. Coppens, J. Eloranta, N. Halberstadt, A. Hernando, D. Mateo, and M. Pi, *Int. Rev. Phys. Chem.* **36**, 621 (2017).
- [17] R. Fröchtenicht, U. Henne, J. P. Toennies, A. Ding, M. Fieber-Erdmann, and T. Drewello, *J. Chem. Phys.* **104**, 2548 (1996).
- [18] M. Joppien, R. Karnbach, and T. Möller, *Phys. Rev. Lett.* **71**, 2654 (1993).
- [19] Karnbach, R. Joppien, M. and Möller, T., *J. Chim. Phys.* **92**, 499 (1995).
- [20] K. von Haeften, A. R. B. d. Castro, M. Joppien, L. Mousavizadeh, R. v. Pietrowski, and T. Möller, *Phys. Rev. Lett.* **78**, 4371 (1997).
- [21] K. von Haeften, T. Laarmann, H. Wabnitz, and T. Möller, *Phys. Rev. Lett.* **88**, 233401 (2002).
- [22] D. S. Peterka, A. Lindinger, L. Poisson, M. Ahmed, and D. M. Neumark, *Phys. Rev. Lett.* **91**, 043401 (2003).
- [23] M. P. Ziemkiewicz, C. Bacellar, K. R. Siefermann, S. R. Leone, D. M. Neumark, and O. Gessner, *J. Chem. Phys.* **141**, 174306 (2014).
- [24] K. D. Closser, O. Gessner, and M. Head-Gordon, *J. Chem. Phys.* **140**, 134306 (2014).
- [25] J. P. Hansen and E. L. Pollock, *Phys. Rev. A* **5**, 2214 (1972).
- [26] M. Rosenblit and J. Jortner, *Phys. Rev. Lett.* **75**, 4079 (1995).
- [27] M. P. Ziemkiewicz, D. M. Neumark, and O. Gessner, *Int. Rev. Phys. Chem.* **34**, 239 (2015).
- [28] O. Kornilov, O. Bünermann, D. J. Haxton, S. R. Leone, D. M. Neumark, and O. Gessner, *J. Phys. Chem.* **115**, 7891 (2011).
- [29] O. Bünermann, O. Kornilov, D. J. Haxton, S. R. Leone, D. M. Neumark, and O. Gessner, *J. Chem. Phys.* **137**, 214302 (2012).
- [30] V. Lyamayev, Y. Ovcharenko, R. Katzy, M. Devetta, L. Bruder, A. LaForge, M. Mudrich, U. Person, F. Stienkemeier, M. Krikunova, T. Möller, P. Piseri, L. Avaldi, M. Coreno, P. O’Keeffe, P. Bolognesi, M. Alagia, A. Kivimäki, M. D. Fraia, N. B. Brauer, M. Drabbels, T. Mazza, S. Stranges, P. Finetti, C. Grazioli, O. Plekan, R. Richter, K. C. Prince, and C. Callegari, *J. Phys. B* **46**, 164007 (2013).
- [31] S. L. Guberman and W. A. Goddard, *Phys. Rev. A* **12**, 1203 (1975).
- [32] A. T. J. B. Eppink and D. H. Parker, *Rev. Sci. Instrum.* **68**, 3477 (1997).
- [33] H. Buchenau, J. P. Toennies, and J. A. Northby, *J. Chem. Phys.* **95**, 8134 (1991).
- [34] A. Hernando, M. Barranco, M. Pi, E. Loginov, M. Langlet, and M. Drabbels, *Phys. Chem. Chem. Phys.* **14**, 3996 (2012).
- [35] J. von Vangerow, A. Sieg, F. Stienkemeier, M. Mudrich, A. Leal, D. Mateo, A. Hernando, M. Barranco, and M. Pi, *J. Phys. Chem. A* **118**, 6604 (2014).
- [36] J. von Vangerow, F. Coppens, A. Leal, M. Pi, M. Barranco, N. Halberstadt, F. Stienkemeier, and M. Mudrich, *J. Phys. Chem. Lett.* **8**, 307 (2017).
- [37] N. V. Dozmorov, A. V. Baklanov, J. von Vangerow, F. Stienkemeier, J. A. M. Fordyce, and M. Mudrich, *Phys. Rev. A* **98**, 043403 (2018).
- [38] D. Mateo, A. Hernando, M. Barranco, E. Loginov, M. Drabbels, and M. Pi, *Phys. Chem. Chem. Phys.* **15**, 18388 (2013).
- [39] P. Y. Serdobintsev, A. S. Melnikov, A. A. Pastor, N. A. Timofeev, and M. A. Khodorkovskiy, *J. Chem. Phys.* **148**, 194301 (2018).
- [40] D. Pentlehner, R. Riechers, B. Dick, A. Slenczka, U. Even, N. Lavie, R. Brown, and K. Luria, *Rev. Sci. Instrum.* **80**, 043302 (2009).
- [41] E. Allaria, R. Appio, L. Badano, W. Barletta, S. Basanese, S. Biedron, A. Borga, E. Busetto, D. Castonovo, Cinquegrana, S. Cleva, D. Cocco, M. Cornacchia, P. Craievich, I. Cudin, G. D’Auria, M. Dal Forno, M. Danailov, R. De Monte, G. De Ninno, P. Delgiusto, A. Demidovich, S. Di Mitri, B. Diviacco, A. Fabris, R. Fabris, W. Fawley, M. Ferianis, E. Ferrari, S. Ferry, L. Froehlich, P. Furlan, G. Gaio, F. Gelmetti, L. Giannessi, M. Giannini, R. Gobessi, R. Ivanov, E. Karantzoulis, M. Lonza, Lutman, B. A. Mahieu, M. Milloch, S. Milton, I. Musardo, M. Nikolov, S. Noe, F. Parmigiani, G. Penco, M. Petronio, L. Pivetta, M. Predonzani, F. Rossi, L. Rumiz, A. Salom, C. Scafuri, C. Serpico, P. Sigalotti, S. Spampinati, C. Spezzani, M. Svandrlik, C. Svetina, S. Tazzari, M. Trovo, R. Umer, A. Vascotto, M. Veronese, R. Visintini, M. Zaccaria, D. Zangrando, and M. Zangrando, *Nat. Photonics* **6**, 699 (2012).
- [42] G. A. Garcia, L. Nahon, and I. Powis, *Rev. Sci. Instrum.* **75**, 4989 (2004).
- [43] H. Koch, O. Christiansen, P. Jørgensen, A. M. Sanchez de Mer’as, and T. Helgaker, *J. Chem. Phys.* **106**, 1808 (1997).
- [44] C. E. Smith, R. A. King, and T. D. Crawford, *J. Chem. Phys.* **122**, 054110 (2005).
- [45] J. M. Turney, A. C. Simmonett, R. M. Parrish, E. Hohenstein, F. Evangelista, J. T. Fermann, B. J. Mintz, L. A. Burns, J. J. Wilke, M. L. Abrams, N. J. Russ, M. L. Leininger, C. L. Janssen, E. T. Seidl, W. D. Allen, H. F. Schaefer, R. A. King, E. F. Valeev, C. D. Sherrill, and T. D. Crawford, *J. Chem. Phys.* **2**, 556 (2012).
- [46] S. L. Fiedler and J. Eloranta, *J. Low Temp. Phys.* **174**, 269 (2014).
- [47] F. Boys and F. Bernardi, *Mol. Phys.* **19**, 553 (1979).
- [48] P. J. Knowles and H.-J. Werner, *Theor. Chim. Acta* **84**, 95 (1992).
- [49] H.-J. Werner, P. J. Knowles, G. Knizia, F. R. Manby, and M. Schütz, *Wiley Interdisciplinary Reviews: Computational Molecular Science* **2**, 242 (2012).
- [50] K. K. Sunil, J. Lin, H. Siddiqui, P. E. Siska, K. D. Jordan, and R. Shepard, *J. Chem. Phys.* **78**, 6190 (1983).
- [51] C. F. Chabalowski, J. O. Jensen, D. R. Yarkony, and B. H. Lengsfeld, *J. Chem. Phys.* **90**, 2504 (1989).